Railroad Bridge Out of Plane Displacement Estimation Using Camera-Laser-IMU System

MAHSA SANEI, PIEDAD MIRANDA and FERNANDO MOREU

ABSTRACT

Transverse displacement, or lateral out-of-plane movement of a railroad bridge, is an important factor in evaluating railroad bridge condition. Excessive movement in this direction can signal potential issues leading to structural failure or an increased risk of derailment. To ensuring the structural stability and safety of railroad bridges, it is critical to monitor the lateral movement of Railroad Bridge. Traditional displacement measurement methods, are usually contact-method often involve complex installation processes that are costly, time-consuming, and pose safety risks, particularly near active train tracks. To address these challenges, this study introduces a non-contact approach for transverse displacement estimation integrating camera, laser, and inertial measurement unit (IMUs). Cameras provide precise position measurements by detecting visible features, while IMUs capture high-frequency movements that cameras may miss. Additionally, camera data corrects drift and long-term errors in IMU readings, improving accuracy. So, to benefit from the strength of both sensor, this study investigate the use of Extended Kalman Filter (EKF) for data fusion and enhancing the estimation accuracy. The effectiveness of this system was evaluated through controlled laboratory experiment simulating bridge pier movements ranging from 1 mm to 25 mm. The UAV movement is simulated in the laboratory considering random translation and rotational movement that may happen because of hovering motion or UAV flying. The system's performance was validated against reference measurements from LVDTs and ground-based laser sensors. Results demonstrated that fusing IMU and camera data yielded more accurate displacement estimates than using camera or laser alone, confirming the advantages of sensor fusion in bridge motion tracking. The developed system will eventually be mounted on a UAV to enable remote and non-contact railroad bridge monitoring, improving accessibility to difficult-to-reach locations. This advancement enhances safety, reduces costs, and increases efficiency in railroad bridge inspections.

INTRODUCTION

Railroad infrastructure in the United States is aging, with over 61,000 railroad bridges exceeding 100 years in service ("ASCE's 2021 American Infrastructure Report Card"). The maintenance and inspection of these structures are critical to ensuring their long-term stability and the safety of the rail network. One of the key indicators of railroad bridge integrity is transverse displacement, which refers to the lateral movement of bridge components under dynamic loading conditions (Moreu et al. 2017). Excessive transverse displacement can signal structural deterioration, which, if left unaddressed, may contribute to service disruptions, safety hazards, and, in extreme cases, failures such as derailments (Li et al. 2019). Therefore, accurate and reliable methods for monitoring railroad bridge displacement are essential for proactive infrastructure management.

Traditional displacement measurement uses contact-based sensors like Linear Variable Differential Transformers (LVDTs) and accelerometers, which, though accurate, require direct installation on the bridge often time-consuming, costly, and impractical in high-traffic or hazardous areas. To address this, recent research

explores non-contact monitoring systems using vision-based methods, inertial measurement units (IMUs), and laser sensors [4], [5].

Vision-based displacement monitoring techniques have gained popularity due to their ability to capture structural movement remotely. These methods use cameras to track visual features on the structure, extracting displacement information using techniques such as feature tracking and optical flow analysis [6].

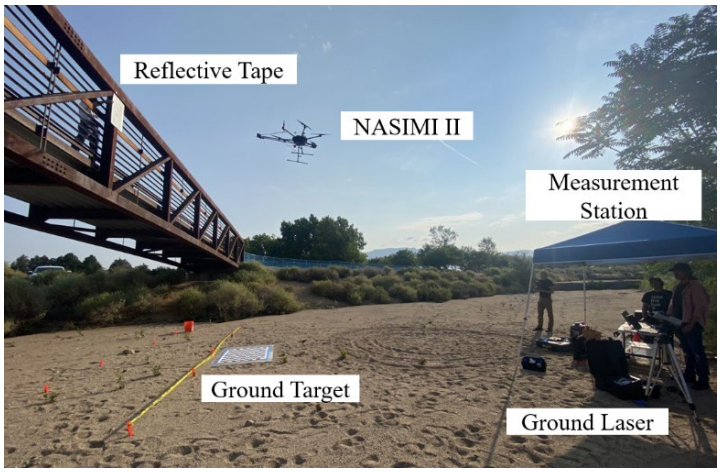

Figure 1. NASIMI II for out-of-plane bridge displacement estimation [7].

However, camera-based methods have limitations, including susceptibility to environmental disturbances such as lighting variations, occlusions, and low frame rates [8]. Similarly, IMU-based approaches provide high-frequency motion tracking, making them well-suited for dynamic displacement monitoring. However, IMUs are prone to long-term drift, where cumulative errors lead to inaccuracies in displacement estimation [9].

To address the limitations of single-sensor approaches, researchers have explored multi-sensor fusion techniques that integrate camera, IMU, and laser data for enhanced displacement monitoring. The Extended Kalman Filter (EKF) has emerged as a widely used framework for fusing sensor data in real-time, allowing for improved accuracy and stability in displacement estimation [10]. EKF-based fusion compensates for the weaknesses of individual sensors, cameras provide position information, IMUs capture high-frequency motion, and lasers offer absolute displacement references, resulting in a more reliable and comprehensive monitoring system [11].

This study proposes a non-contact, UAV-compatible system for railroad bridge displacement monitoring, integrating a laser, camera, and IMU within an EKF-based fusion framework. The objective is to improve the accuracy of transverse displacement estimation while addressing the limitations of traditional contact-based and single-sensor methods.

METHODOLOGY

General

The EKF algorithm used for displacement estimation follows a prediction-correction cycle to iteratively update the system state based on sensor inputs.

Video Processing

The algorithm starts with processing video frames to estimate the displacement and orientation of a camera relative to a checkerboard pattern as it explained in the (Nasimi & Moreu 2021) (w/o fusion). The camera tracks the UAV's movement using the pinhole camera model, which maps 3D world coordinates to 2D image coordinates through intrinsic and extrinsic parameters obtained during calibration. For the checkerboard pattern tracking, the relative position between the camera (UAV) and the target structure has to be determined. Given a 3D point in world coordinates (X_w, Y_w, Z_w) its projection onto the image plane as pixel coordinates (u, v) is given by equation (1).

$$\begin{bmatrix} u \\ v \\ 1 \end{bmatrix} = K \begin{bmatrix} R & T \end{bmatrix} \begin{bmatrix} X_w \\ Y_w \\ Z_w \\ 1 \end{bmatrix} \tag{1}$$

where K is the intrinsic parameters of the camera, and [R T] corresponds to each frame rotational matrix and translational vector.

IMU-Camera Data Fusion

The algorithm initializes the EKF state vector, $\mathbf{x}$= $[p_x, p, p_z, v_x, v_y, v_z, \Psi, \phi, \theta]$ for position, velocity, and Euler angles, along with the initial covariance and noise parameters. Motion updates are then predicted using IMU readings based on the process model in equation (2).

$$f(\boldsymbol{x}, \boldsymbol{u}, \Delta t) = \begin{bmatrix} p_x + v_x \Delta t + \frac{1}{2} a_x \Delta t^2 \\ p_y + v_y \Delta t + \frac{1}{2} a_y \Delta t^2 \\ p_z + v_z \Delta t + \frac{1}{2} a_z \Delta t^2 \\ v_x + a_x \Delta t \\ v_y + a_y \Delta t \\ v_z + a_z \Delta t \\ \Psi + g_x \Delta t \\ \phi + g_y \Delta t \\ \theta + g_z \Delta t \end{bmatrix} \tag{2}$$

The nonlinear process model is linearized using the Jacobian matrix F, enabling the EKF to propagate the state covariance matrix P via equation (3).

$$P_{pred} = FPF^T + Q \tag{3}$$

w here Q represents the process noise covariance. During the update step, the EKF refines the predicted state using camera measurements of displacement and orientation. The Kalman Gain K, which weights the new measurement, is computed using equation (4).

$$K = P_{pred} H^T (H P_{pred} H^T + R)^{-1} \tag{4}$$

where H is the Jacobian of the measurement function, and R is the measurement noise covariance matrix. The updated state is then calculated using equation (5).

$$\mathbf{x}_{new} = \mathbf{x}_{pred} + K(\mathbf{z} - h(\mathbf{x}_{pred})) \tag{5}$$

Here, z is the actual measurement from the camera, and $h(\mathbf{x}_{pred})$ is the predicted measurement based on $\mathbf{x}_{pred}$. This equation updates the state vector by incorporating the measurement z and the residual $\mathbf{z} - h(\mathbf{x}_{pred})$ using equation (6).

$$P_{new} = (I - KH)P_{old} \tag{6}$$

Where I is the identity matrix, updating the state covariance after incorporating the measurement. The next step is to correct this measurement with obtained displacement from the laser.

Laser Correction

The laser is used to measure the relative displacement D_L between the UAV and the bridge structure while the fusion of camera and IMU data captures UAV motion. To obtain the corrected transverse displacement D_c, the effect of orientation angles is accounted for using equation (7).

$$D_c = D_L . \cos\phi . \cos\theta \tag{7}$$

where D_L is the raw displacement measured by the laser. The total transverse displacement $D_t(t)$ is then computed by adjusting for UAV movement using equation (8).

$$D_t(t) = -[(D_c(t) - D_c(t_0)) - (D_{UAV}(t) - D_{UAV}(t_0))] \tag{8}$$

EXPERIMENT

A laboratory experiment was conducted to measure the out-of-plane displacement of a simulated railroad bridge pier using a camera, laser, and IMU. These sensors were mounted on a carbon bar, which was securely attached to a hexapod platform capable of moving in six degrees of freedom (DOF).

A downward-facing phone camera recorded video of a checkerboard pattern with 20 mm squares for calibration, while an IMU and laser were also attached to the carbon bar to capture both rotational and translational movements. A wooden board was manually moved to simulate bridge vibrations, with an LVDT sensor and a Polytec RSV-150 laser recording its displacement as ground truth with 1000Hz sampling rate. The test lasted approximately 30 seconds, collecting data to validate the system before its application to real-world bridge monitoring with a UAV. The experiment setup is shown in Figure 2.

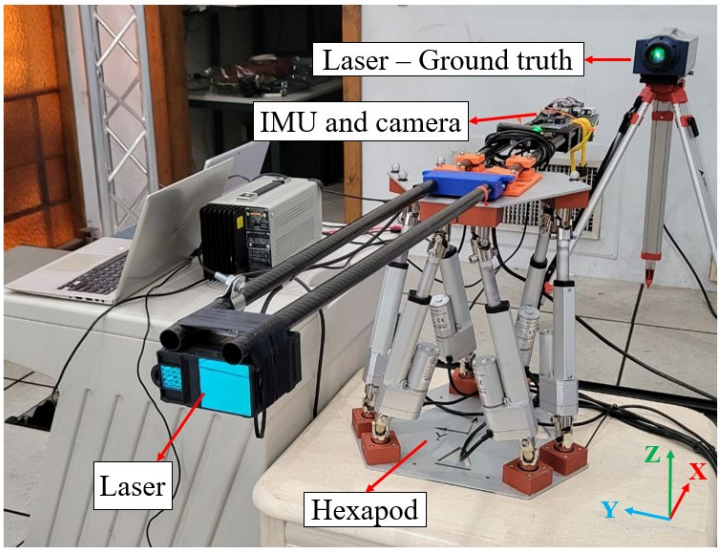

Figure 2. Experiment setup.

A hexapod platform is used to simulate the UAV movement in order to enable the team to replicate the experiment many times with different UAV trajectory and simulate the realistic outdoor environmental factors such as wind. In this study, the hexapod platform was used to generate controlled displacements, simulating a scenario with randomly generated translations and rotations within a range of 1 inch for translation and 3 degrees for rotation. Figure 3 presents the input .csv file used by the hexapod, along with the corresponding output, which serves as the input for the algorithm.

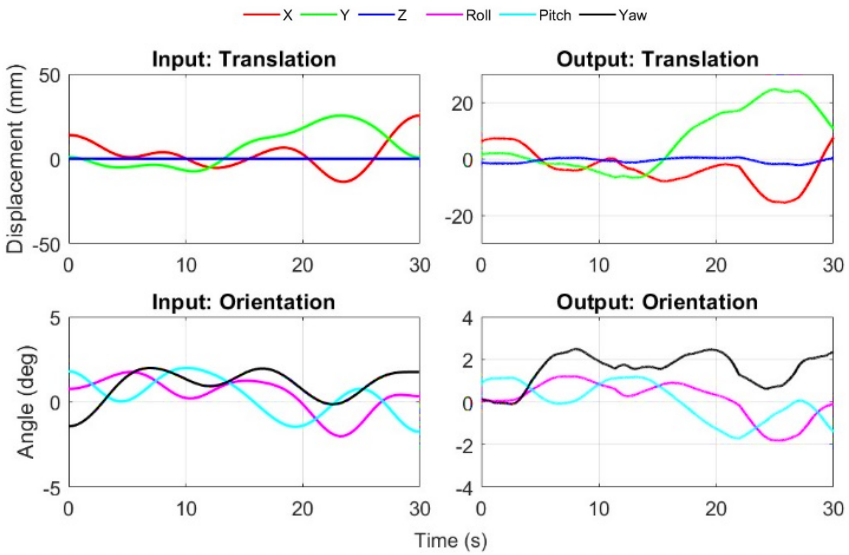

Figure 3. Test input (left) and output (right) from hexapod.

RESULTS AND DISCUSSION

The effectiveness of the proposed camera-laser-IMU fusion system was evaluated using contact sensor (LVDT). Figure 4 shows the estimated displacement with fusion,

which is the focus of this study, and without fusion, which is the method used in [12], compared to the ground truth data.

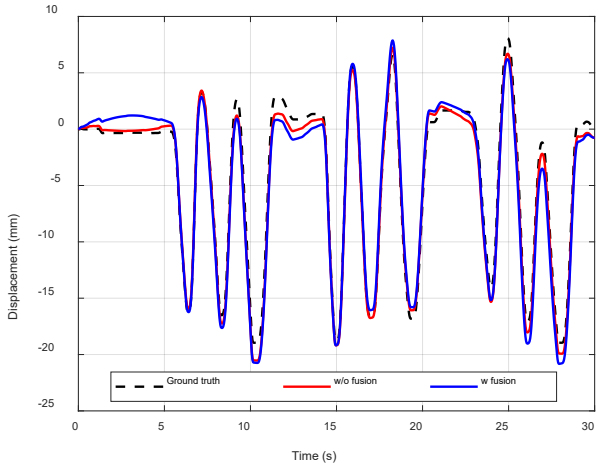

Figure 4. Estimated displacement with and without fusion compared to ground truth.

The system's performance was assessed using key error metrics, including Peak Error, and Root Mean Square Error. These metrics quantify the accuracy of displacement estimation under different motion conditions using equation (9) and (10).

$$Peak\ error = \max(|\Delta e_i - \Delta m_i| \tag{9}$$

$$RMSE = \sqrt{\frac{1}{N}\sum_{i=1}^{N}(\Delta e_i - \Delta m_i)^2} \tag{10}$$

Where Δe_i is the displacement estimated by the proposed method, Δm_i is the displacement measured by the reference sensor and N is the total number of data points. When a train crosses a bridge, the structure moves in different directions which is important since it can signal structural problems or even pose a derailment risk. Peak-to-peak displacement captures the full range of this movement by measuring the distance between the highest and lowest points during a cycle. Engineers rely on these measurements to assess bridge health, check structural models, and ensure the bridge is operating safely. The peak-to-peak displacement is calculated with and without fusion and compared with the ground-truth peak-to-peak values.

The peak-to-peak error trends in the Figure 5 illustrate that measurement accuracy varies over time, with non-fused estimates generally showing higher errors than fused estimates. There are a few distinct error peaks such as the first peak-to-peak error suggests that specific UAV motion conditions may contribute to these fluctuations.

TABLE I. ERROR COMPARISON

Index	Peak error (mm)	RMSE (mm)	Peak-to-peak error (mm)
w/o fusion	5.45	3.04	0.7
w fusion	1.78	0.87	0.25

Table I presents a quantitative comparison of displacement estimation errors with and without applying the sensor fusion algorithm, under controlled UAV-like motion

simulated by a hexapod platform. The platform introduced randomized translations (up to 1 inch) and rotations (up to 3 degrees) to replicate realistic flight dynamics affected by environmental disturbances like wind. The results clearly demonstrate the advantage of using sensor fusion. The peak error dropped from 5.45 mm to 1.78 mm, representing a 67% improvement. Similarly, the RMSE decreased by approximately 71%, from 3.04 mm to 0.87 mm, indicating enhanced overall tracking consistency. The peak-to-peak error, which reflects the range of oscillations in displacement estimation, was reduced by 64%, from 0.7 mm to 0.25 mm. These reductions suggest that the fusion algorithm not only improves the accuracy of individual displacement estimates but also significantly stabilizes the signal, making it more resilient to noise and motion-induced disturbances. This validates the effectiveness of the fusion method in capturing realistic UAV movements with high precision. Figure 5 shows the peak-to-peak errors for all nine peaks in each of the displacement time history.

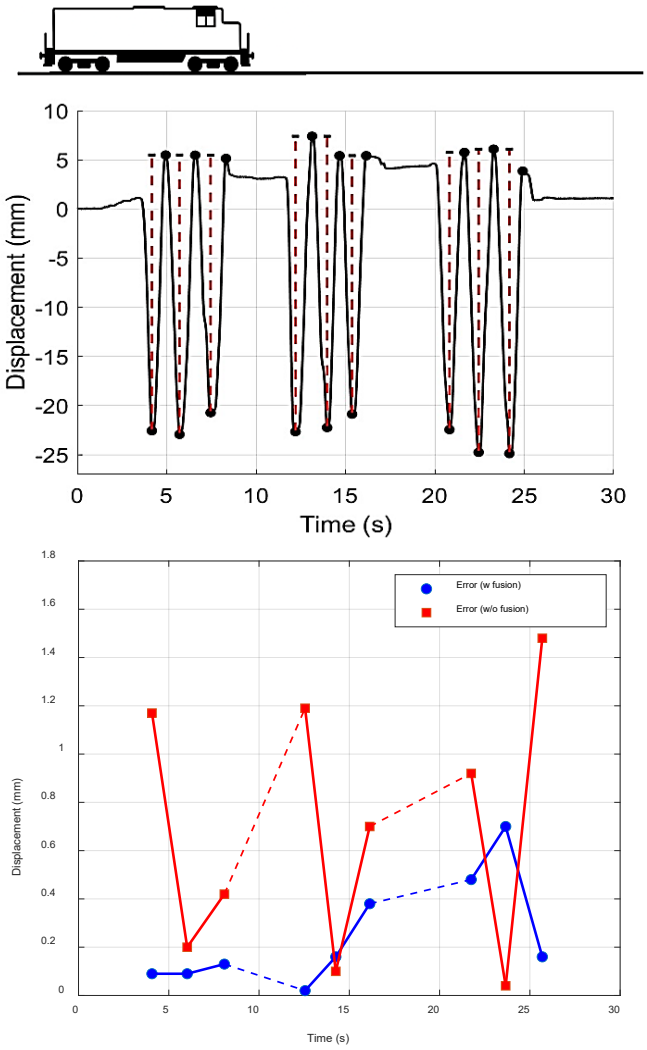

Figure 5. Peak-to-peak error analysis.

CONCLUSION

This study presented a novel non-contact method for monitoring railroad bridge displacement. This is a practical alternative to traditional sensing methods, especially in situations where inspectors cannot physically access a bridge to install sensors. The ground truth displacement with estimated algorithm with and without fusion showed that integration of these sensors with an Extended Kalman Filter improved measurement accuracy by approximately 68%, reducing errors associated with individual sensor limitations. Future work will focus on optimizing the system for UAV deployment in real-world Bridge monitoring applications. This approach can support railroad infrastructure owners in safely and efficiently collecting displacement data without relying on fixed reference points.

REFERENCES

1. "ASCE's 2021 American Infrastructure Report Card," ASCE's 2021 Infrastructure Report Card |. Accessed: Oct. 11, 2024. [Online]. Available: https://infrastructurereportcard.org/
2. F. Moreu, R. E. Kim, and B. F. Spencer Jr., "Railroad bridge monitoring using wireless smart sensors," *Structural Control and Health Monitoring*, vol. 24, no. 2, p. e1863, 2017, doi: 10.1002/stc.1863.
3. C. Li, L. Yu, and S. Fei, "Real-Time 3D Motion Tracking and Reconstruction System Using Camera and IMU Sensors," *IEEE Sensors Journal*, vol. 19, no. 15, pp. 6460–6466, Aug. 2019, doi: 10.1109/JSEN.2019.2907716.
4. R. Nasimi and F. Moreu, "Development and Implementation of a Laser–Camera–UAV System to Measure Total Dynamic Transverse Displacement," *Journal of Engineering Mechanics*, vol. 147, no. 8, p. 04021045, Aug. 2021, doi: 10.1061/(ASCE)EM.1943-7889.0001939.
5. H. Sekiya, K. Kimura, and C. Miki, "Technique for Determining Bridge Displacement Response Using MEMS Accelerometers," *Sensors*, vol. 16, no. 2, Art. no. 2, Feb. 2016, doi: 10.3390/s16020257.
6. D. Hester, J. Brownjohn, M. Bocian, and Y. Xu, "Low cost bridge load test: Calculating bridge displacement from acceleration for load assessment calculations," *Engineering Structures*, vol. 143, pp. 358–374, Jul. 2017, doi: 10.1016/j.engstruct.2017.04.021.
7. R. Nasimi, F. Moreu, and G. M. Fricke, "Sensor Equipped UAS for Non-Contact Bridge Inspections: Field Application," *Sensors*, vol. 23, no. 1, Art. no. 1, Jan. 2023, doi: 10.3390/s23010470.
8. S. Jang *et al.*, "Structural Health Monitoring of a Cable-Stayed Bridge Using Smart Sensor Technology: Deployment and Evaluation," *Smart Structures and Systems*, vol. 6, Jul. 2010, doi: 10.12989/sss.2010.6.5_6.439.
9. D. Ribeiro, R. Calçada, J. Ferreira, and T. Martins, "Non-contact measurement of the dynamic displacement of railway bridges using an advanced video-based system," *Engineering Structures*, vol. 75, pp. 164–180, Sep. 2014, doi: 10.1016/j.engstruct.2014.04.051.
10. R. Nasimi, F. Moreu, M. Nasimi, and R. Wood, "Developing Enhanced Unmanned Aerial Vehicle Sensing System for Practical Bridge Inspections Using Field Experiments," *Transportation Research Record*, vol. 2676, no. 6, pp. 514–522, Jun. 2022, doi: 10.1177/03611981221075618.
11. Y. Zhao, Y. Liang, Z. Ma, L. Guo, and H. Zhang, "Localization and Mapping Algorithm Based on Lidar-IMU-Camera Fusion," *Journal of Intelligent and Connected Vehicles*, vol. 7, no. 2, pp. 97–107, Jun. 2024, doi: 10.26599/JICV.2023.9210027.
12. R. Nasimi and F. Moreu, "A methodology for measuring the total displacements of structures using a laser–camera system," *Computer-Aided Civil and Infrastructure Engineering*, vol. 36, no. 4, pp. 421–437, 2021, doi: 10.1111/mice.12652.